

Local structural evolutions of CuO/ZnO/Al₂O₃ catalyst for methanol synthesis under operando conditions studied by in situ quick X-ray absorption spectroscopy

Xue-Ping Sun^{1,2} · Fan-Fei Sun¹ · Song-Qi Gu¹ · Jing Chen¹ · Xian-Long Du¹ · Jian-Qiang Wang¹ · Yu-Ying Huang¹ · Zheng Jiang¹

Received: 2 September 2016 / Revised: 21 October 2016 / Accepted: 25 October 2016 / Published online: 26 December 2016
© Shanghai Institute of Applied Physics, Chinese Academy of Sciences, Chinese Nuclear Society, Science Press China and Springer Science+Business Media Singapore 2016

Abstract In situ quick X-ray absorption spectroscopy (QXAFS) at the Cu and Zn K-edge under operando conditions has been used to unravel the Cu/Zn interaction and identify possible active site of CuO/ZnO/Al₂O₃ catalyst for methanol synthesis. In this work, the catalyst, whose activity increases with the reaction temperature and pressure, was studied at calcined, reduced, and reacted conditions. TEM and EDX images for the calcined and reduced catalysts showed that copper was distributed uniformly at both conditions. TPR profile revealed two reduction peaks at 165 and 195 °C for copper species in the calcined catalyst. QXAFS results demonstrated that the calcined form consisted mainly of a mixed CuO and ZnO, and it was progressively transformed into Cu metal particles and dispersed ZnO species as the reduction treatment. It was demonstrated that activation of the catalyst precursor occurred via a Cu⁺ intermediate, and the active catalyst predominantly consisted of metallic Cu and ZnO even

under higher pressures. Structure of the active catalyst did not change with the temperature or pressure, indicating that the role of the Zn was mainly to improve Cu dispersion. This indicates the potential of QXAFS method in studying the structure evolutions of catalysts in methanol synthesis.

Keywords In situ · Quick X-ray absorption spectroscopy · CuO/ZnO/Al₂O₃ catalyst · Operando condition

1 Introduction

Due to rapid industrial developments and enhanced human activities, carbon dioxide levels in the atmosphere have reached approximately 400 ppm for the first time in history [1]. Converting CO₂ into useful feedstock chemicals and fuels is an important strategy for removing CO₂ from the atmosphere and for reducing our dependence on petrochemicals [2–4]. Among the products derived from CO₂, methanol is a basic chemical as a feedstock for producing formaldehyde, olefin, and other products [5]. In 2005, Olah et al. initiated a “methanol economy” concept [6, 7]. According to this proposal, methanol can serve as an efficient energy-storage chemical and a fuel substitute [8, 9]. Therefore, methanol synthesis through carbon dioxide hydrogenation has attracted worldwide research interest in the past 20 years [10–17].

In investigations of low-pressure process for methanol synthesis using CuO/ZnO/Al₂O₃ catalyst, which began in the late 1960s, there exist different opinions on the nature of active sites and the role of promoters [18–21]. Some researchers pointed out the metallic copper atoms were uniformly active for methanol synthesis [22, 23]. For example, Pan et al. [24] found that the activity of the

This work was supported by the National Basic Research Program of China (973 Program, 2013CB933104) and the National Natural Science Foundation of China (Nos. 11275258 and 11135008).

Electronic supplementary material The online version of this article (doi:10.1007/s41365-016-0170-y) contains supplementary material, which is available to authorized users.

✉ Yu-Ying Huang
huangyuying@sinap.ac.cn

✉ Zheng Jiang
jiangzheng@sinap.ac.cn

¹ Shanghai Institute of Applied Physics, Chinese Academy of Sciences, Zhangjiang Campus, Shanghai 201204, China

² University of Chinese Academy of Sciences, Beijing 100049, China

catalyst was directly proportional to the surface area of metallic Cu. Deng et al. [25] also reported that the catalytic activity of a CuO/ZnO/Al₂O₃ catalyst for carbon dioxide hydrogenation increased with the surface area of metallic copper, reached a maximum, and then decreased at a Cu/ZnO molar ratio of 8. However, in the presence of CO₂ and with a fraction of the Cu⁰ surface covered by oxygen-containing species, the catalytic activity toward methanol synthesis no longer depended on the Cu⁰ surface area [26, 27]. This was explained that the Cu⁺ sites might be active sites in methanol synthesis. Herman et al. [28] found that active Cu⁺ ion sites were dissolved on the surface of the ZnO matrix. Synergetic effect between copper and the promoter was reported by several groups [29, 30]. Fujitani and Nakamura [31] proposed the creation of a Cu–Zn surface alloy on active sites. Herman et al. [28] indicated that the catalytic magnitude was greater than that of the pure copper metal or zinc oxide, bearing the consequence of the synergistic interaction between copper and ZnO.

In general, the formation of active sites is analyzed after quenching the treated samples. It is important to directly follow the operando structural changes in catalyst by using an in situ method. For better understanding the active sites and the promoter effect in the catalysts, synchrotron-based X-ray absorption fine structure (XAFS) and its two main modifications, X-ray absorption near edge structure (XANES) and extended X-ray absorption fine structure (EXAFS), are well suited to the local structural investigation in catalytic research [32–36]. In addition, in situ XAFS is a premier tool for dynamically monitoring the structural evolutions of catalyst under operando conditions, which has been used by many researchers attempting to understand the active site formation during preparation, activation, and reaction process [37–40].

In this work, we prepared a CuO/ZnO/Al₂O₃ catalyst by an oxalate gel co-precipitation method and investigated the structural information of the CuO/ZnO/Al₂O₃ catalyst at operando conditions by in situ quick XAFS (QXAFS) method [41]. Unlike the usual step-scan method, the monochromator in QXAFS is continuously moved in the quick mode. It is possible to detect the comprehensive changes in a short time, providing direct insight for understanding the copper state and the promotion effects in CuO/ZnO/Al₂O₃ catalyst.

2 Experimental section

2.1 Preparation of catalyst

CuO/ZnO/Al₂O₃ catalyst was synthesized by an oxalate gel co-precipitation method [42]. Mixed zinc nitrate, copper nitrate and aluminum nitrate (all from Aldrich, 99.999%),

and 20% excess of oxalic acid were dissolved in ethanol individually. The two solutions were mixed at room temperature by using a peristaltic pump. The precipitate was separated by centrifuge and dried overnight at 110 °C. Then, it was calcined at 400 °C for 4 h in a muffle oven. Subsequently, the CuO/ZnO/Al₂O₃ catalyst was obtained. The metal loading of the catalyst determined by inductively coupled plasma atomic emission spectroscopy amounted to CuO/ZnO/Al₂O₃ (36.80% ± 0.5wt%/Cu, 37.90% ± 0.5wt%/Zn, 3.50% ± 0.5wt%/Al).

2.2 Catalytic test

The CuO/ZnO/Al₂O₃ catalyst (1.0 g, 60–80 mesh) mixed with quartz sand (2.0 g, 60–80 mesh) was loaded in the isothermal zone of a fixed-bed reactor. After the catalyst was reduced with pure H₂ at 250 °C (1 bar) for 4 h, the temperature was decreased to 200 °C, and the mixture gas (3 H₂/1 CO₂) (with 0.1 N₂ as internal standard) was cut in. It was performed at 1 bar and 10 bar with the gas hourly space velocity (GHSV, h⁻¹) of 3000. The same scheme was followed at 250 °C and 300 °C. A hot trap (100 °C) and a cold trap (2–4 °C) were sequentially set at downstream of the reactor to collect liquid products. The liquid products were analyzed by using an Agilent 7820A gas chromatograph equipped with a capillary column INNOWAX (30 m × 0.25 mm) and a flame ionization detector. Gas-phase products were collected in a gas bag and were analyzed by using an Agilent GC (7820A) equipped with a Porapak Q and 5A packed column and a thermal conductivity detector.

2.3 TEM characterization

Transmission electron microscope (TEM) images were obtained using a FEI Tecnai G2 F20 SS-TWINTeM operated at 220 kV. The CuO/ZnO/Al₂O₃ catalyst was dispersed ultrasonically in ethanol and loaded onto a copper grid.

2.4 TPR measurement

The reduction behavior of the CuO/ZnO/Al₂O₃ catalyst was tested by temperature-programmed reduction (H₂-TPR, Micromeritics AutoChem II 2920). The catalyst was loaded into a U-tube and treated by a helium flow at 200 °C for 1 h. After the catalyst was cooled down to 50 °C, the gas flow was switched from helium to 5% H₂/Ar mixtures. The temperature was increased to 500 °C in the rate of 5 °C/min. The H₂ consumption was monitored by a thermal conductivity detector (TCD) throughout the whole reduction process.

2.5 QXAFS measurement

QXAFS measurements were performed at Beamline BL14W1 at the Shanghai Synchrotron Radiation Facility (SSRF), operated at 3.5 GeV, and Beamline 1W1B of the Beijing Synchrotron Radiation Facility (BSRF) operated at 2.2 GeV. High-order harmonics were successfully inhibited by using a harmonic suppression mirror. Transmission mode was performed both at the Cu K-edge and at the Zn K-edge. Two gas-filled ionization chambers were used to measure the intensities of the incident beam (I_0) and the transmitted beam (I_1) after the sample. The gas used in the chambers depended upon the element being examined. The CuO/ZnO/Al₂O₃ catalyst was mixed with BN and finely ground to obtain an appropriate absorption edge jump. It was then centered in a homemade XAFS cell. Detail information for the cell is given in Sect. 3.4.1.

Firstly, initial states of the catalyst at the Cu K-edge and Zn K-edge were collected. Next, the whole in situ reduction treatment was performed at 150 °C (10% H₂/He, 1 bar), and the gas flow was kept at 10 ml/min. Then, the temperature was up to 200 °C, and the reducing gas was switched to the mixture of 3H₂/1CO₂ (1 bar). After that, increasing the temperature (at 5 °C/min) and pressure to 300 °C and 5 bar, respectively, at the gas flow of 50 mL/min, the XAFS data were collected continuously and each QXAFS scan took just 60 s. Finally, the XAFS data were analyzed using the software package of Iffeffit. Phase shifts and backscattering amplitudes used for the data analysis were obtained from spectra of the reference compounds of Cu-foil, CuO, Cu₂O, Zn-foil and ZnO. The $\chi(k)$ data were multiplied by k^3 to compensate the of EXAFS oscillation damping in the high k -region. Fourier transformation (FT) from k -space to R -space was performed, and all the EXAFS data were fitted in R -space. From the analysis, structural parameters, such as the coordination numbers (N), bond distance (R), Debye–Waller factor and inner potential shift, could be calculated.

3 Results and discussion

3.1 Catalytic test

The catalytic activity and selectivity for methanol synthesis on the CuO/ZnO/Al₂O₃ catalyst are listed in Table 1. According to the reaction thermodynamics, temperature has an important effect on the activity performance. The results show that the CO₂ conversion increases with the temperature. However, the methanol yield at 250 °C is greater than that at 300 °C. As the methanol synthesis reaction is an exothermic reaction, the selectivity of methanol decreases with increasing temperatures, accompanied by increasing

Table 1 Activity performances of CuO/ZnO/Al₂O₃ catalyst in methanol synthesis reaction

| Conditions | C _{CO₂} ^a (%) | S _{CH₃OH} ^b (%) | S _{CO} ^c (%) | Y _{CH₃OH} ^d (%) |
|-----------------|--|--|----------------------------------|--|
| 1 bar (200 °C) | 7.3 | 32.7 | 67.3 | 2.4 |
| 1 bar (250 °C) | 12.6 | 23.4 | 76.6 | 2.9 |
| 1 bar (300 °C) | 17.9 | 14.6 | 85.4 | 2.6 |
| 10 bar (200 °C) | 10.6 | 43.3 | 56.7 | 4.6 |
| 10 bar (250 °C) | 17.8 | 29.5 | 70.5 | 5.3 |
| 10 bar (300 °C) | 21.9 | 15.7 | 84.3 | 3.4 |

^a CO₂ conversion. ^b Selectivity of CH₃OH. ^c Selectivity of CO. ^d CH₃OH yield

CO selectivity. Therefore, the lower methanol yield is due to the limitation of thermodynamic equilibrium. Both the CO₂ conversion and methanol yield at 10 bar are greater than those at 1 bar at the same temperatures. Obviously, the activity performance is significantly affected by the thermodynamics effect.

3.2 TEM characterization

TEM images and EXD elemental mappings of the calcined catalyst and reduced catalyst are shown in Fig. 1. The EDX mappings show uniform distributions of copper on both catalyst samples, indicating that zinc oxide can improve copper dispersion in the CuO/ZnO/Al₂O₃ catalyst. Therefore, a morphology effect is always postulated to the role of the zinc oxide in a Cu-based catalyst that ZnO may optimize dispersion of the Cu particles and stabilize the active sites by attenuating the unavoidable agglomeration of Cu particles [43]. The particle size distributions estimated are shown in Fig. 2. The average particle sizes of the calcined and the reduced catalysts are 7.6 and 8.2 nm, respectively.

3.3 TPR analysis

In order to investigate the reduction behavior of the catalyst, TPR measurement was performed. Figure 3 shows the reduction profiles of the CuO/ZnO/Al₂O₃ catalyst and CuO reference. The peak at 260 °C in bulk CuO is attributed to the reduction of CuO to metallic Cu, while the reduction temperature of the CuO/ZnO/Al₂O₃ catalyst was obviously lower than that of the reference CuO, with a major peak at 195 °C and a shoulder peak at 165 °C, which could be related to the reduction of bulk CuO and highly dispersed CuO species, respectively [44, 45]. The difference of TPR profiles between the reference CuO and CuO/ZnO/Al₂O₃ catalyst indicates the interaction of Cu species with promoter ZnO. This is in line with the results of TEM.

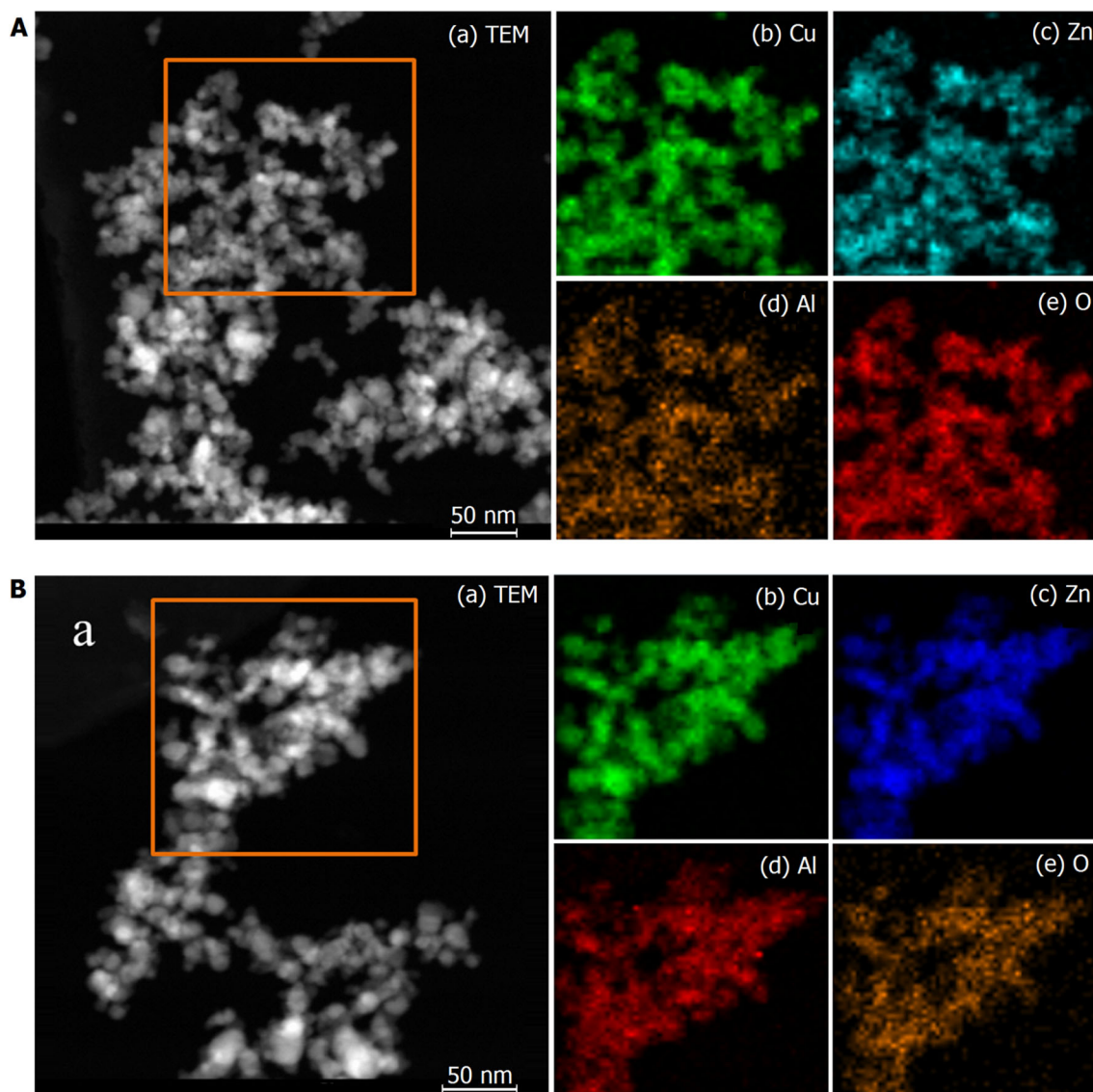


Fig. 1 TEM image (a) and EDX elemental mappings (b–e) of the calcined (A) and reduced (B) CuO/ZnO/Al₂O₃ catalysts

3.4 XAFS analysis

3.4.1 The design of the *in situ* XAFS cell

The actual working chemical state and local geometric structure of Cu and Zn were studied with *in situ* XAFS measurements, as fingerprints to identify the structural state at different stages. Figure 4 shows a new type of *in situ* XAFS cell we designed. Its four windows are of binder-less polycrystalline boron nitride, a new material for X-ray windows with desirable purity, chemical and thermal stability, and the second hardest materials next to diamond. The BN windows are 2 μm thick, which can endure high pressures and allow sufficient transmittance for X-ray even at 5 keV. Made of stainless steel, the *in situ* cell consists of a heating system, a cooling system, and a gas system.

Temperatures of the central body, ranging from liquid nitrogen to 500 $^{\circ}\text{C}$, are monitored by thermocouples. Its pressure ranges from vacuum to 0.6 MPa. It allows both transmission and fluorescence modes. The catalyst was held inside the reactor using a stainless-steel holder (Fig. 4b).

3.4.2 Calcined CuO/ZnO/Al₂O₃ catalyst

Figure 5 shows the Cu K-edge and Zn K-edge XANES spectra for the Cu/ZnO/Al₂O₃ catalyst and, for comparison, the spectra of Cu, Cu₂O, CuO, Zn, and ZnO. As the transition energy depends on the ion charge, the edge position shifted toward lower energies with oxidation states: 8980.0, 8981.1, and 8984.3 eV for Cu, Cu₂O, and CuO, respectively. The Cu K-edge XANES spectra in Fig. 5a are

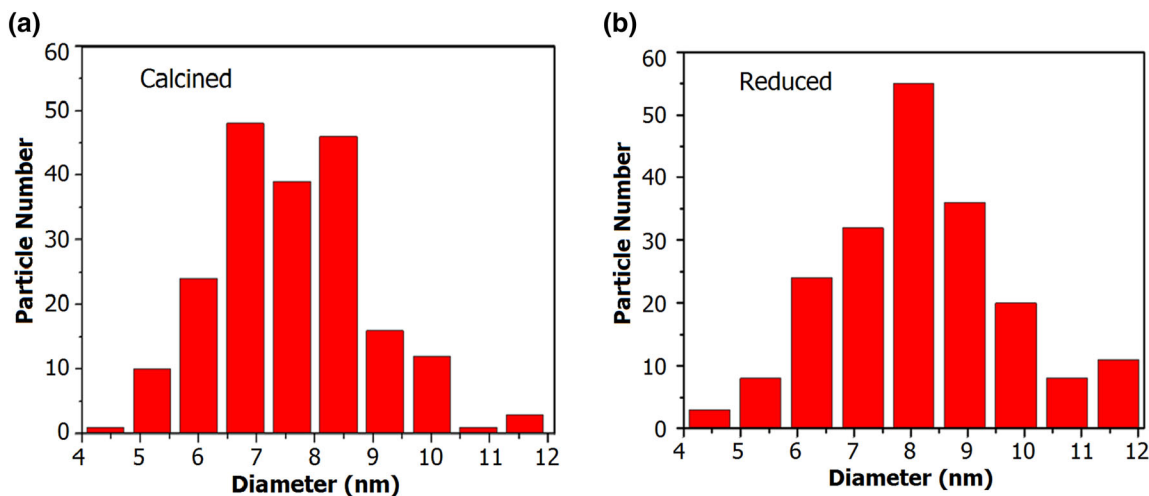


Fig. 2 Particle size distributions of calcined **a** and reduced **b** CuO/ZnO/Al₂O₃ catalysts

clearly related to the CuO reference in terms of edge position and features. Figure 5b exhibits the zinc K-edge XANES profile in the calcined CuO/ZnO/Al₂O₃ catalyst. An edge position and features are similar to those of the

ZnO reference. A main peak located at 9669 eV with a shoulder at 9663 eV can be assigned to the Zn²⁺ dipole-allowed electron transition relative to 1s-4p^{a,b} and 1s-4p^c, respectively [39].

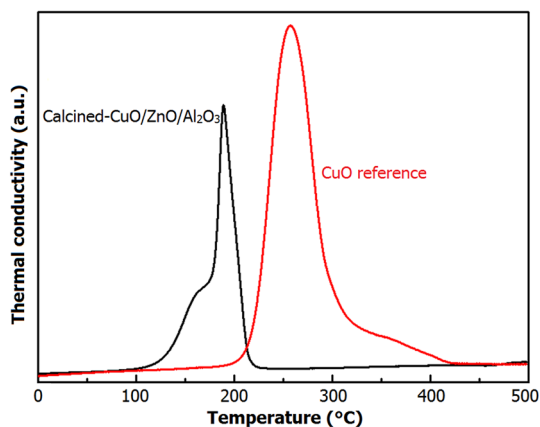


Fig. 3 H₂-TPR profiles of the calcined CuO/ZnO/Al₂O₃ catalyst and the CuO reference

3.4.3 Reduction behavior of CuO/ZnO/Al₂O₃ catalyst by QXAFS

QXAFS spectra were collected continuously in an entire in situ process. From the TPR results in Sect. 3.3, Cu²⁺ was gradually reduced by hydrogen at 160 °C, while zinc oxide was stable even at 500 °C. In order to follow the detailed structural change in copper species, we performed the QXAFS measurement at 150 °C and controlled a lower gas flow at 10 mL/min. However, probably due to the low temperature and low gas flow, no obvious change was observed for the first 20 min of the reduction process. Therefore, the XANES data in Fig. 6a were shown 20 min later. Figure 6b shows composition changes in the catalyst, obtained by the linear combination fitting analysis. The percentage of Cu²⁺ at initial state was 100%, which was in

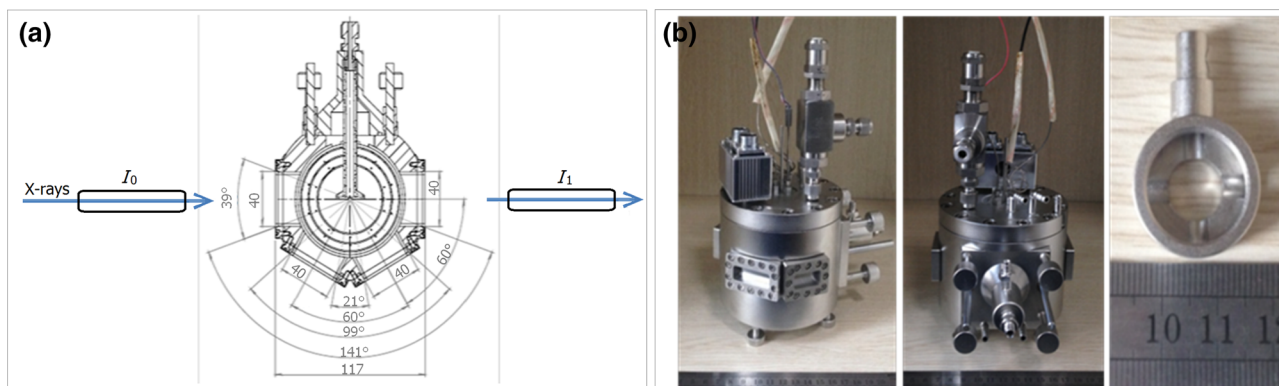


Fig. 4 In situ XAFS cell. **a** Schematics in transmission mode; **b** details of the setup

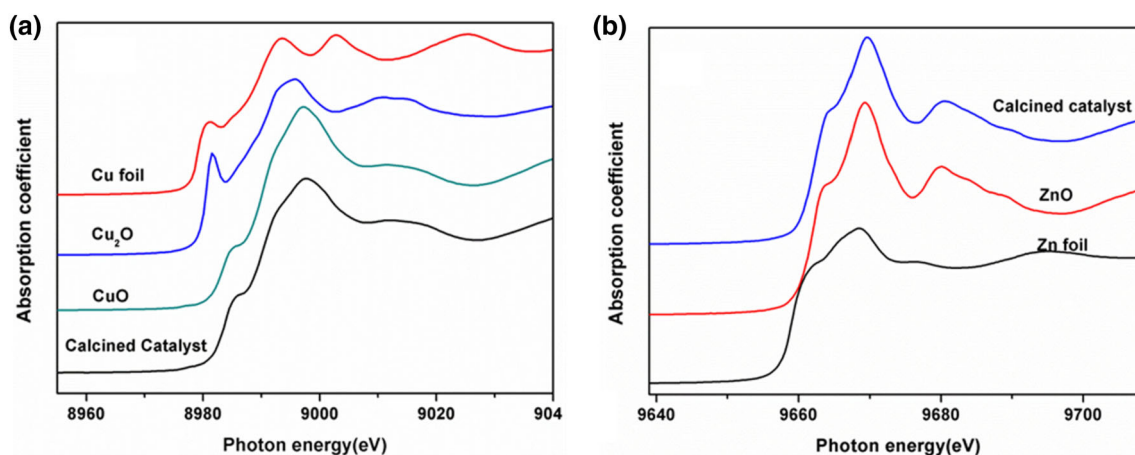


Fig. 5 Cu K-edge XANES spectra **a** and Zn K-edge XANES spectra **b** for the calcined CuO/ZnO/Al₂O₃ catalyst

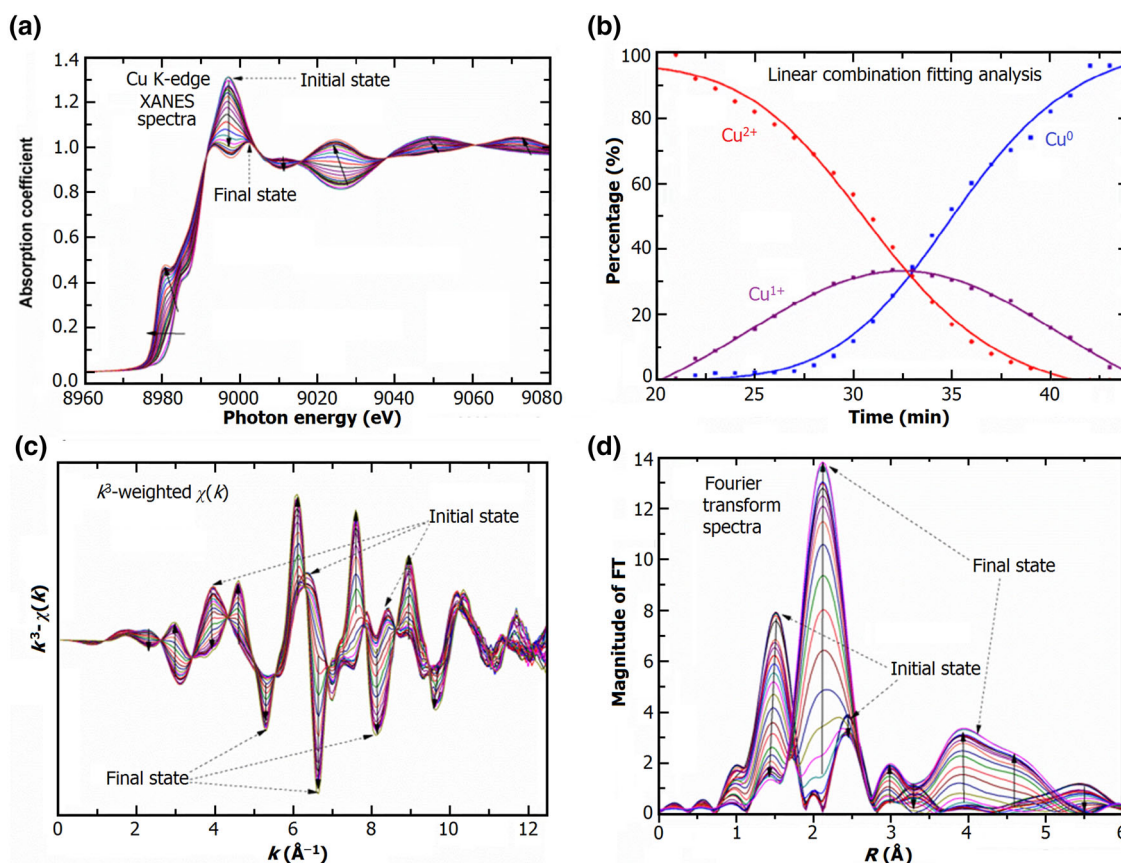


Fig. 6 Cu K-edge XANES spectra **a**, the linear combination fitting analysis **b**, the corresponding k^3 -weighted $\chi(k)$ data **c** and Fourier transform spectra **d** for the calcined catalyst measured under 10% H₂/He flow at 150 °C

line with the analysis result in Fig. 5a. In the reduction process, the edge position and the white line of the Cu K-edge XANES remarkably decreased. Cu⁺ and Cu⁰ phases were detected, resulting from reduction of Cu²⁺. The absence of peak in 8984.3 eV was attributed to the 1s–4p transition in Cu²⁺, and the presence of peak in 8980 eV was attributed to the 1s–4p transition in Cu⁰. The final stage was characterized by an almost complete depletion of

CuO and the presence of Cu metallic phase. All the copper atoms got reduced by longer reduction time. In addition, the presence of Cu⁺ could be observed as the intermediate in the reduction process by QXAFS method.

The corresponding k^3 -weighted $\chi(k)$ data and Fourier transform spectra are shown in Fig. 6c, d, respectively. The peak around 1.5 and 2.5 Å without phase-corrected Fourier transforms in Fig. 6d corresponded to an O shell and Cu–

Cu (O) shell, respectively. Both peaks decreased gradually with increasing reduction time, while a new peak attributed to the Cu–Cu metallic bond increased with the reduction time. The results of the in situ QXAFS experiment correlated well with other reports that the Cu²⁺ was gradually reduced to Cu⁰ [44].

3.4.4 In situ XAFS study under reaction conditions for CuO/ZnO/Al₂O₃ catalyst

Figure 7a, b shows the Cu K-edge and Zn K-edge XANES spectra of the CuO/ZnO/Al₂O₃ catalyst during different reaction treatments. There are no obvious changes in the XANES spectra of copper and zinc. This indicates that the active phases on CuO/ZnO/Al₂O₃ catalyst are stable. Figure 7c shows the corresponding Fourier-transformed spectra for the catalyst. The main peak around 2.2 Å without phase-corrected Fourier transforms corresponded to Cu–Cu metallic shell, and the lower intensity of the peaks at higher distances indicates the increasing disorder effect in the catalyst. The main peaks at different

temperatures in Fig. 7c do not differ significantly in shape, except for a noticeable variation in the amplitude and bond distance. According to our previous studies [46–48], the slight changes could be induced by the increasing disorder effect.

Due to the large disorder effect of the catalyst at higher temperatures, data analysis using the conventional Gaussian mode can result in erroneously results [45]. To account for the deviation from the harmonic behavior, the cumulant expansion technique was used to correct the error in bond contraction. The EXAFS fitting results are given in Table 2. Generally, error bounds (accuracies) that characterize the structural parameters obtained from EXAFS spectra are estimated at $N = \pm 20\%$ and $R = \pm 1\%$. The main peak with the coordination number of ~ 11.0 at 2.54 Å corresponded to the Cu–Cu contribution. It was similar to that of bulk Cu by considering the error bounds in N . For zinc (in supporting information Table S1), the first and second peaks corresponded to Zn–O and Zn–Zn (O), respectively. The coordination numbers for them were similar with that of bulk ZnO with tetrahedral structure

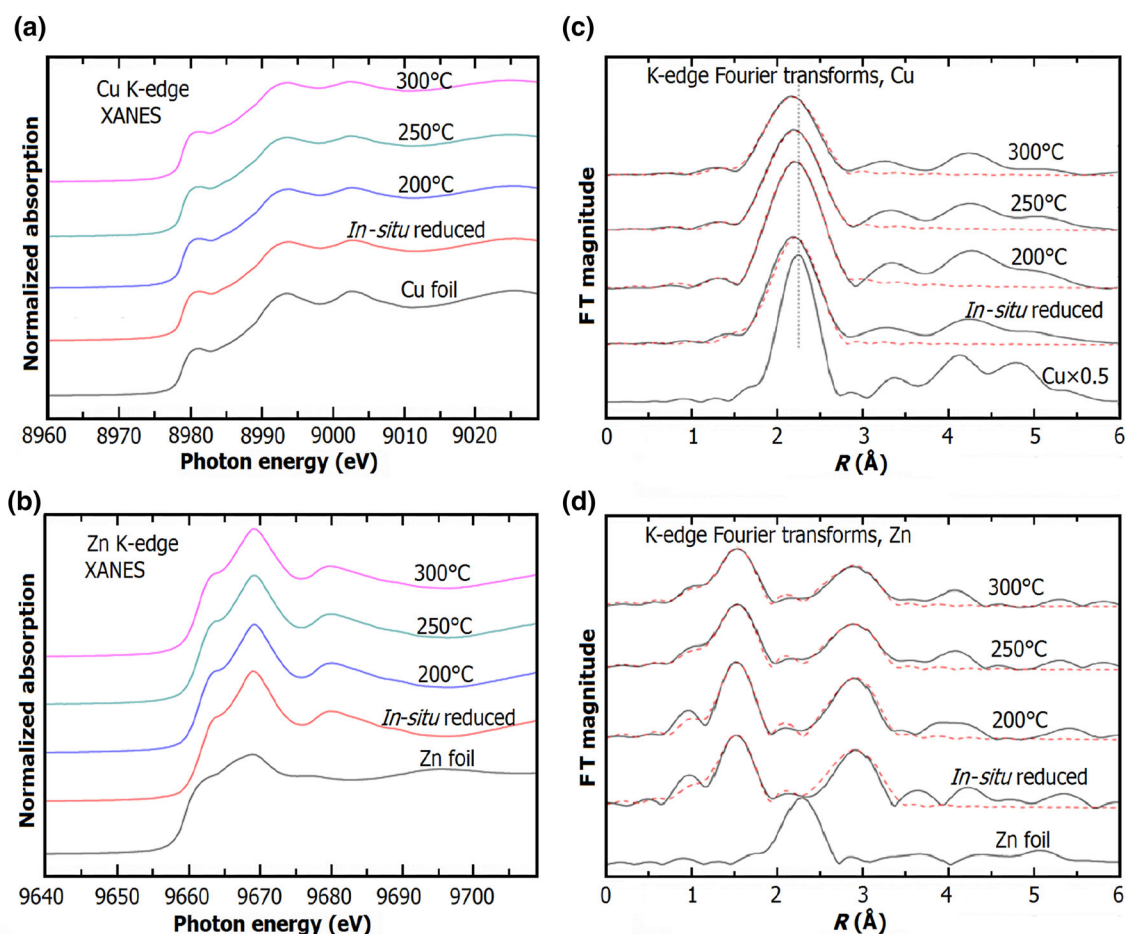


Fig. 7 CuO/ZnO/Al₂O₃ catalyst under different reaction conditions (3H₂/1CO₂, 5 bar) compared with the foil references. **a, b** K-edge XANES spectra, **c** and **d** corresponding Fourier transforms magnitudes with the corresponding fitting curve (dotted line)

Table 2 EXAFS fit parameters for Cu

| Sample | Path | <i>N</i> | <i>R</i> (Å) | ΔE_0 (eV) | $\Delta\sigma^2$ (Å ²) | $\Delta\sigma_7^2$ (Å ²) [41] | $\Delta\sigma_s^2$ (Å ²) | <i>R</i> -factor (%) |
|-----------|-------|-------------|---------------|-------------------|------------------------------------|---|--------------------------------------|----------------------|
| Cu-foil | Cu–Cu | 12 | 2.55 | −1.0 (±0.3) | 0.013 (±0.001) | 0.0026 | 0.011 | 0.0031 |
| Cu 200 °C | Cu–Cu | 10.9 (±1.1) | 2.54 (±0.025) | −2.6 (±1.5) | 0.014 (±0.001) | 0.0035 | 0.011 | 0.0058 |
| Cu 250 °C | Cu–Cu | 10.9 (±1.1) | 2.54 (±0.025) | −2.6 (±1.5) | 0.015 (±0.001) | 0.0040 | 0.011 | 0.0057 |
| Cu 300 °C | Cu–Cu | 10.8 (±0.4) | 2.54 (±0.053) | 1.9 (±1.6) | 0.016 (±0.003) | 0.0043 | 0.011 | 0.0091 |

N, coordination number; *R*, interatomic distance; σ , disorder parameter; ΔE_0 , energy shift. The fitting analyses were performed in the *R* space. $\Delta R = 1.0$ – 3.0 and $\Delta K = 2.94$ – 10.0 . $S_0^2 = 0.87$ was obtained from fitting the Cu-foil (Fm-3 m space group). C_3 was calculated at 0.002

[39]. No obvious changes could be observed in the coordination numbers and the bond distance of copper and zinc at different temperatures. This is in line with the XANES results, while the Debye–Waller factors for all contribution bonds gradually become stronger.

From the micro-perspective, the atomic thermal motion increases with the sample temperature, which increases the mean square variation of each scattering path length, and the σ_T indicates the inherent properties of atoms which can only be affected by the temperature. In order to explain the real state of the structural change (σ_S), the disorder factor was divided into σ_T and σ_S by the Einstein model. The σ_T can be obtained from the fitting results of CuO/ZnO/Al₂O₃ under nitrogen atmosphere [45]. Therefore, the structural disorder (σ_S) obtained is given in Table 2. The structural disorder was 0.0011. The active catalyst consisted of mainly metallic Cu and ZnO, and the active catalyst structure did not change with temperature. Therefore, the role of the zinc oxide in CuO/ZnO/Al₂O₃ catalyst can be postulated to a morphology effect that optimizes and stabilizes the dispersion of the Cu particles.

4 Conclusion

In situ XAFS method allows detailed and exhaustive structural characterization of the CuO/ZnO/Al₂O₃ catalyst under operation conditions. QXAFS data can be recorded under different gas mixtures at different temperatures and pressures. It is demonstrated that activation of the catalyst precursor occurs via a Cu⁺ intermediate, and the active catalyst consists of mainly metallic Cu and ZnO, and the active catalyst structure does not change with temperature or pressure, indicating that the ZnO improves Cu dispersion. This study brings new insights into the complex and dynamic changes in different in situ treatments.

References

1. Mauna Loa Observatory, Hawaii. [http://co2now.org/\(2014\)](http://co2now.org/(2014))

2. K.M.K. Yu, I. Curcic, J. Gabriel et al., Recent advances in CO₂ capture and utilization. *Chem. Sus. Chem.* **1**, 893–899 (2008). doi:10.1002/cssc.201090023
3. W. Wang, S.P. Wang, X.B. Ma et al., Recent advances in catalytic hydrogenation of carbon dioxide. *Chem. Soc. Rev.* **40**, 3703–3727 (2011). doi:10.1039/c1cs15008a
4. G. Centi, E.A. Quadrelli, S. Perathoner, Catalysis for CO₂ conversion: a key technology for rapid introduction of renewable energy in the value chain of chemical industries. *Energy Environ. Sci.* **6**, 1711–1731 (2013). doi:10.1039/C3EE00056G
5. G.A. Olah, G.K.S. Prakash, A. Goepfert, Anthropogenic chemical carbon cycle for a sustainable future. *J. Am. Chem. Soc.* **133**, 12881–12898 (2011). doi:10.1021/ja202642y
6. G.A. Olah, *Jenseits von öl und Gas: die Methanolwirtschaft*. *Angew. Chem.* **117**, 2692–2696 (2005). doi:10.1002/ange.200462121
7. G.A. Olah, Beyond oil and gas: the methanol economy. *Angew. Chem. Int. Ed.* **44**, 2636–2639 (2005). doi:10.1002/anie.200462121
8. P. Gao, F. Li, F.K. Xiao et al., Effect of hydrotalcite-containing precursors on performance of Cu/Zn/Al/Zr catalysts for CO₂ hydrogenation: introduction of Cu²⁺ at different formation stages of precursors. *Catal. Today* **194**, 9–15 (2012). doi:10.1016/j.cattod.2012.06.012
9. U. Olsbye, S. Svelle, M. Bjørgen et al., Conversion of methanol to hydrocarbons: how zeolite cavity and pore size controls product selectivity. *Angew. Chem.* **51**, 5810–5831 (2012). doi:10.1002/aine.201103657
10. E.E. Ortelli, J. Wambach, A. Wokaun, Methanol synthesis reactions over CuZr based catalyst investigated using periodic variations of reaction concentrations. *Appl. Catal. A* **216**, 227–241 (2001). doi:10.1016/S0926-860X(01)00569-5
11. A.K. Shukla, P.A. Christensen, A.J. Dickinson et al., A liquid-feed solid polymer electrolyte direct methanol fuel cell operating at near-ambient conditions. *J. Power Sources* **76**, 54–59 (1998). doi:10.1016/S0378-7753(98)00140-2
12. G.C. Chinchin, K.C. Waugh, D.A. Whan, The activity and state of the copper surface in methanol synthesis catalysts. *Appl. Catal.* **25**, 101–107 (1986). doi:10.1016/S0166-9834(00)81226-9
13. F. Liao, Y.Q. Huang, J.W. Ge et al., Morphology-dependent interactions of ZnO with Cu nanoparticles at the materials' interface in selective hydrogenation of CO₂ to CH₃OH. *Angew. Chem.* **123**, 2210–2213 (2011). doi:10.1002/anie.201007108
14. P. Gao, F. Li, H.J. Zhan et al., Influence of Zr on the performance of Cu/Zn/Al/Zr catalysts via hydrotalcite-like precursors for CO₂ hydrogenation to methanol. *J. Catal.* **298**, 51–60 (2013). doi:10.1016/j.jcat.2012.10.030
15. M. Behrens, F. Studt, I. Kasatkin et al., The active site of methanol synthesis over Cu/ZnO/Al₂O₃ industrial catalysts. *Science* **336**, 893–897 (2012). doi:10.1126/science.1219831
16. Y.Q. Cen, X.N. Li, H.Z. Liu, Preparation of copper-based catalysts for methanol synthesis by acid-alkali-based alternate

- precipitation method. *Chin. J. Catal.* **27**, 210–216 (2006). doi:[10.1016/S1872-2067\(06\)60014-4](https://doi.org/10.1016/S1872-2067(06)60014-4)
17. J.J. Wu, X.D. Zhou, Catalytic conversion of CO₂ to value added fuels: current status, challenges, and future directions. *Chin. J. Catal.* **37**, 999–1015 (2016). doi:[10.1016/S1872-2067\(16\)62455-5](https://doi.org/10.1016/S1872-2067(16)62455-5)
 18. J. Nakamura, Y. Choi, T. Fujitani, On the issue of the active site and the role of ZnO in Cu/ZnO methanol synthesis catalysts. *Top. Catal.* **22**, 277–285 (2003). doi:[10.1023/A:1023588322846](https://doi.org/10.1023/A:1023588322846)
 19. J.D. Grunwaldt, A.M. Molenbroek, N.Y. Topsøe, H. Topsøe, In situ investigations of structural changes in Cu/ZnO catalysts. *J. Catal.* **194**(45), 452–460 (2000). doi:[10.1006/jcat.2000.2930](https://doi.org/10.1006/jcat.2000.2930)
 20. T. Fujitani, J. Nakamura, The effect of ZnO in methanol synthesis catalysts on Cu dispersion and the specific activity. *Catal. Lett.* **56**, 119–124 (1998). doi:[10.1023/A:1019000927366](https://doi.org/10.1023/A:1019000927366)
 21. L. Dong, X.J. Yao, Y. Chen, Interactions among supported copper based catalyst components and their effects on performance: a review. *Chin. J. Catal.* **34**, 851–864 (2013). doi:[10.1016/S1872-2067\(12\)60592-0](https://doi.org/10.1016/S1872-2067(12)60592-0)
 22. B. Denise, R.P.A. Sneed, B. Beguin et al., Supported copper catalysts in the synthesis of methanol: N₂O-titrations. *Appl. Catal.* **30**, 353–358 (1987). doi:[10.1016/S0166-9834\(00\)84125-1](https://doi.org/10.1016/S0166-9834(00)84125-1)
 23. T.H. Fleisch, R.L. Micicille, Studies on the chemical state of Cu during methanol synthesis. *J. Catal.* **90**, 165–171 (1984). doi:[10.1016/0021-9517\(84\)90099-X](https://doi.org/10.1016/0021-9517(84)90099-X)
 24. W.X. Pan, R. Cao, D.L. Roberts et al., Methanol synthesis activity of Cu/ZnO catalysts. *J. Catal.* **114**, 440–444 (1988). doi:[10.1016/0021-9517\(88\)90047-4](https://doi.org/10.1016/0021-9517(88)90047-4)
 25. J.F. Deng, Q. Sun, Y.L. Zhang et al., A novel process for preparation of a Cu/ZnO/Al₂O₃ ultrafine catalyst for methanol synthesis from CO₂ + H₂: comparison of various preparation methods. *Appl. Catal. A* **139**, 75–80 (1996). doi:[10.1016/0926-860X\(95\)00324-X](https://doi.org/10.1016/0926-860X(95)00324-X)
 26. G.C. Chinchin, K.C. Waugh, D.A. Whan, The activity and state of the copper surface in methanol synthesis catalysts. *Appl. Catal.* **25**, 48–51 (1986). doi:[10.1016/S0166-9834\(00\)81226-9](https://doi.org/10.1016/S0166-9834(00)81226-9)
 27. G.C. Chinchin, M.C. Spencer, K.C. Waugh et al., Promotion of methanol synthesis and the water-gas shift reactions by adsorbed oxygen on supported copper catalysts. *J. Chem Soc Faraday Trans. I* **83**, 2193–2200 (1987). doi:[10.1039/F19878302193](https://doi.org/10.1039/F19878302193)
 28. R.G. Herman, K. Klier, G.W. Simmons et al., Catalytic synthesis of methanol from COH₂: I. Phase composition, electronic properties, and activities of the Cu/ZnO/M₂O₃ catalysts. *J. Catal.* **56**, 407–410 (1979). doi:[10.1016/0021-9517\(79\)90132-5](https://doi.org/10.1016/0021-9517(79)90132-5)
 29. H.Y. Chen, S.P. Lau, L. Chen et al., Synergism between Cu and Zn sites in Cu/Zn catalysts for methanol synthesis. *Appl. Surf. Sci.* **152**, 193–198 (1999). doi:[10.1016/S0169-4332\(99\)00317-7](https://doi.org/10.1016/S0169-4332(99)00317-7)
 30. Y. Kanai, T. Watanabe, T. Fujitani et al., The synergy between Cu and ZnO in methanol synthesis catalysts. *Catal. Lett.* **38**, 157–163 (1996). doi:[10.1007/BF00806562](https://doi.org/10.1007/BF00806562)
 31. T. Fujitani, J. Nakamura, The chemical modification seen in the Cu/ZnO methanol synthesis catalysts. *Appl. Catal. A* **191**, 111–129 (2000). doi:[10.1016/S0926-860X\(99\)00313-0](https://doi.org/10.1016/S0926-860X(99)00313-0)
 32. D.E. Sayers, E.A. Stern, F.W. Lytle, New technique for investigating noncrystalline structures: Fourier analysis of the extended X-ray absorption fine structure. *Phys. Rev. Lett.* **27**, 1204–1207 (1971). doi:[10.1103/PhysRevLett.27.1204](https://doi.org/10.1103/PhysRevLett.27.1204)
 33. J. Singh, C. Lamberti, J.A. Bokhoven, Advanced X-ray absorption and emission spectroscopy: in situ catalytic studies. *Chem. Soc. Rev.* **39**, 4754–4766 (2010). doi:[10.1039/c0cs00054j](https://doi.org/10.1039/c0cs00054j)
 34. H.L. Bao, X.P. Sun, J. Zheng et al., Structural changes of Rh-Mn nanoparticles inside carbon nanotubes studied by X-ray absorption spectroscopy. *Chin. J. Catal.* **35**, 1418–1427 (2014). doi:[10.1016/S1872-2067\(14\)60081-4](https://doi.org/10.1016/S1872-2067(14)60081-4)
 35. A.E. Russell, A. Rose, X-ray absorption spectroscopy of low temperature fuel cell catalysts. *Chem. Rev.* **104**, 4613–4635 (2004). doi:[10.1002/chin.200450216](https://doi.org/10.1002/chin.200450216)
 36. H.S. Yu, X.J. Wei, J. Li et al., The XAFS beamline of SSRF. *Nucl. Sci. Tech.* **26**, 050102 (2015). doi:[10.13538/j.1001-8042/nst.26.050102](https://doi.org/10.13538/j.1001-8042/nst.26.050102)
 37. K. Evgeny, S. Jacinto, A.D. Jehad et al., Structure of the methanol synthesis catalyst determined by in situ HERFD XAS and EXAFS. *Catal. Sci. Technol.* **2**, 373–378 (2012). doi:[10.1039/c1cy00277e](https://doi.org/10.1039/c1cy00277e)
 38. S. Velu, K. Suzuki, C.S. Gopinath et al., XPS, XANES and EXAFS investigations of CuO/ZnO/Al₂O₃/ZrO₂ mixed oxide catalysts. *Phys. Chem. Chem. Phys.* **4**, 1990–1999 (2002). doi:[10.1039/b109766k](https://doi.org/10.1039/b109766k)
 39. D. Grandjean, V. Pelipenko, E.D. Batyrev et al., Dynamic Cu/Zn interaction in SiO₂ supported methanol synthesis catalysts unraveled by in-situ XAFS. *J. Phys. Chem. C* **115**, 20175–20191 (2011). doi:[10.1021/jp201839s](https://doi.org/10.1021/jp201839s)
 40. J. Fang, F.C. Shi, H.Z. Bao et al., Evolution of surface and bulk structures of Ce_xTi_{1-x}O₂ oxide composites. *Chin. J. Catal.* **34**, 2075–2083 (2013). doi:[10.1016/S1872-2067\(12\)60667-6](https://doi.org/10.1016/S1872-2067(12)60667-6)
 41. K. Okumura, T. Honma, S. Hirayama et al., Stepwise growth of Pd clusters in USY zeolite at room temperature analyzed by QXAFS. *J. Phys. Chem. C* **112**, 16740–16747 (2008). doi:[10.1021/jp804381c](https://doi.org/10.1021/jp804381c)
 42. Q. Sun, Y.L. Zhang, H.Y. Chen et al., A novel process for the preparation of Cu/ZnO and Cu/ZnO/Al₂O₃ ultrafine catalyst: structure, surface properties, and activity for methanol synthesis from CO₂ + H₂. *Chin. J. Catal.* **167**, 92–105 (1997). doi:[10.1006/jcat.1997.1554](https://doi.org/10.1006/jcat.1997.1554)
 43. J. Yoshihara, C.T. Campbell, Methanol synthesis and reverse water-gas shift kinetics over Cu(110) model catalysts: structural sensitivity. *J. Catal.* **161**, 776–782 (1996). doi:[10.1006/jcat.1996.0240](https://doi.org/10.1006/jcat.1996.0240)
 44. X.S. Dong, F. Li, N. Zhao et al., CO₂ hydrogenation to methanol over Cu/ZnO/ZrO₂ catalysts prepared by precipitation-reduction method. *Appl. Catal. B* **191**, 8–17 (2016). doi:[10.1016/j.apcatb.2016.03.014](https://doi.org/10.1016/j.apcatb.2016.03.014)
 45. Z. Li, H.Y. Zheng, K.C. Xie, Surface properties of CuO/ZnO/Al₂O₃ catalyst for methanol synthesis in slurry reactor. *Chin. J. Catal.* **29**, 431–435 (2008). doi:[10.3321/j.issn:0253-9837.2008.05.005](https://doi.org/10.3321/j.issn:0253-9837.2008.05.005)
 46. X.P. Sun, F.F. Sun, Z.H. Sun et al., Disorder effects on EXAFS modeling for catalysts working at elevated temperatures. *Radiat. Phys. Chem.* (2016). doi:[10.1016/j.radphyschem.2016.01.039](https://doi.org/10.1016/j.radphyschem.2016.01.039)
 47. A. Yevick, A.I. Frenkel, Effect of surface disorder on EXAFS modeling of metallic clusters. *Phys. Rev. B* **81**, 760–762 (2010). doi:[10.1103/PhysRevB.81.115451](https://doi.org/10.1103/PhysRevB.81.115451)
 48. E.B. Batyrev, J.C.V.D. Heuvel, J. Beckers et al., The effect of the reduction temperature on the structure of Cu/ZnO/SiO₂ catalysts for methanol synthesis. *J. Catal.* **229**, 136–143 (2005). doi:[10.1016/j.jcat.2004.10.012](https://doi.org/10.1016/j.jcat.2004.10.012)